



## **RESISTANCE SPOT WELDING OF DISSIMILAR METALS AISI 1006 LOW CARBON STEEL AND AA6061 ALUMINUM ALLOY USING ZINC AND TIN COATING**

**Ammar Yasir Akkar<sup>1</sup>, Muhaed Alali<sup>2</sup>**

**1 MSc student, Materials Engineering, Department Faculty of Engineering, University of Kufa, Najaf, Iraq. Email: [ammaryasir.akar.35@gmail.com](mailto:ammaryasir.akar.35@gmail.com)**

**2 Assistant Professor, Materials Engineering, Department Faculty of Engineering, University of Kufa, Najaf, Iraq. Email: [mowahid.alali@uokufa.edu.iq](mailto:mowahid.alali@uokufa.edu.iq)**

**[HTTPS://DOI.ORG/10.30572/2018/KJE/140301](https://doi.org/10.30572/2018/KJE/140301)**

### **ABSTRACT**

In this research, low carbon steel (AISI 1006) and aluminum (AA6061) were joined by resistance spot welding. Different types of coating for the base metals were used to examine their influence on the properties of the welded joint. A tensile shear test for the welded joints was performed to determine the best welding conditions. low welding current produced an interfacial failure mode, and the failure mode changed from interfacial to partial pullout and full pullout failure modes with increasing welding current. For the as-welded joints, the best welding condition was 6 kA, 0.6 s, and the joint recorded a shear force of 2.7 kN. The shear force increased to 4.24 kN for the tin-coated steel / zinc-coated aluminum joint. The microstructure examination showed the welding made through a brazing mechanism. However, the existence of the Fe-Al intermetallic compound (IMC) caused a cracking at the joint interface. The microhardness of the joint was affected by the heat of welding and varied across the joint. An increase in the microhardness of aluminum in the weld nugget occurred because of the IMC.

**KEYWORDS:** Dissimilar welding, Resistance Spot welding, Coating, Intermetallic compounds, Failure type.

## 1. INTRODUCTION

Dissimilar material welding aided in bringing the benefits of two materials together, often providing solutions for engineering needs in terms of decreasing weight and boosting properties (Manh, 2016). Aluminium to carbon steel welding is significant because aluminium/steel joints have a low density of aluminium combined with the higher tensile strength of steel both of which have desired properties for engineering applications (Rajesh et al., 2014). However, welding of aluminium to steel presents some difficulties due to the different thermal and physical properties of both metals, aluminium expulsion, the presence of porosities at the weld interface, and the formation of thick brittle Al/Fe intermetallic compounds (IMCs) (Rahimi and Movahedi, 2020). Regarding IMCs, while they are important in achieving efficient contact between Aluminum and steel, excessive growth of the IMC leads to a joint fragility (Chen *et al.*, 2018). Resistance spot welding (RSW) is one of the common techniques to join aluminium to steel owing to its high efficiency, cheap cost, flexibility, and widespread application in comparable metal joining in the automated manufacturing (Chen *et al.*, 2019). The bonding zone length, which is defined as the width of a liquid aluminum nugget, and the thickness of the IMC layer are some of the parameters that govern the mechanical characteristics of Al/steel RSW joint. The IMCs are a substantial contributor to the brittleness of the metallic junction since they typically display very poor plastic deformability. Their result, reducing the thickness of the IMC layer as much as possible is essential for getting acceptable mechanical characteristics (Gullino *et al.*, 2019). In order to solve this issue, intermediate interlayers were used in the welding of dissimilar metals. These interlayers were able to effectively avoid the formation of brittle IMCs. Additionally, the interlayer may help reduce the thermal expansion mismatch between the substrates while the weld is being performed (Fang *et al.*, 2019). To avoid the growth of brittle IMCs, several interlayers were utilized, such as aluminum-coated steel, pure aluminum, aluminum-magnesium alloy, aluminum-copper alloy, copper coating, and aluminum-silicon alloy. More recent studies have looked at how zinc coating affects the weldability of aluminum/steel (Das, Tanmoy et al., 2020; Azhari-Saray, Hamed et al., 2020). In order to provide a strong weld between steel and aluminum, a zinc coating is often used. This coating increases the wettability of the steel's surface to molten aluminum during the welding (Singh, Arora and Shukla, 2019). There is another method that improves the heat conduction control interface between IMCs by adding a cover plate to the surface of the aluminum plate. The resistance spot welding connections made of aluminum and steel have been strengthened significantly thanks to these techniques (Ren, Daxin, 2018). This research aims to study the weldability between AA6061 and low carbon steel joints welded by the RSW technique. The

test samples of Al/steel welds were generated by different combinations of welding current and time. Cover plate and metallic coating of Zn and Sn were also utilized to study their effect on joint mechanical properties and improve the weldability between the two dissimilar metals.

## 2. EXPERIMENTAL WORK

### 2.1. Materials and methods

As base metals, thin sheets of (AA6061) aluminum alloy and (AISI 1006) low-carbon steel were used. The thickness of the aluminum sheets was 1.6 mm, and the carbon steel was 0.8 mm. This variation in sheet thickness provides some heat balance to the welding joint due to the difference in thermal properties between steel and aluminum as illustrated in Table 1. The chemical composition of the base metals is illustrated in Tables 2 and 3. To form a standard lap joint for the tensile shear test in accordance with EN ISO 14273, the sheets were cut into specimens with dimensions of (105×30 mm). The specimens were then joined as in the configuration shown in Fig 1. Metallic coatings of zinc and tin were applied to both materials. The electrolytic technique was used for the zinc coating on AA6061, and the sheet of AA6061 was cleaned to remove any surface contamination that might have been present. Then, the sample was submerged in nitric acid HNO<sub>3</sub> (50 percent by volume) at room temperature for two minutes, then rinsed with water. Then, the sample was dipped in zincate at 35 °C for two minutes. During the process of tin coating for AISI 1006, the electroplating technique was used. Any surface contamination was removed from sheets of AISI 1006 steel. The sample was immersed in a diluted hydrochloric acid (1:3) solution, then rinsed with water. Then, the sample was dipped in a container of tin solution heated to 50 °C for two minutes.

**Table 1. Physical properties of low carbon steel and AA6061**(Šut'ák *et al.*, 2020) (Sharma *et al.*, 2022).

<b>Material</b>	<b>Melting °C</b>	<b>Thermal conductivity (W.m-1.K-1)</b>	<b>Thermal expansion (m.m-1.K-1)</b>
Low carbon steel	1540	64	12*10 <sup>-6</sup>
AA6061	558	151-202	2.32*10 <sup>-5</sup>

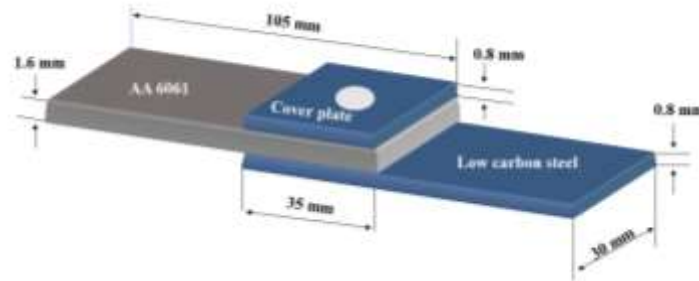
**Table 2. The chemical compositions analysis of AA6061 (Prabakaran *et al.*, 2017).**

Elements wt.%	Si%	Fe%	Cu%	Mn%	Mg%	Cr%	Zn%	Ti%	Al%
Standard	0.4- 0.8	Max. 0.7	0.15- 0.40	Max. 0.15	0.8- 1.2	0.04- 0.35	Max. 0.25	Max. 0.15	Balance
Obtained	0.703	0.477	0.251	0.131	0.909	0.193	0.0343	0.0757	97.2

**Table 3. The chemical compositions analysis of AISI 1006 steel.**

Elements wt%	C%	Si%	Mn%	P%	S%	Cr%	Mo%	Ni%	Fe%
Standard	0.08	-	0.25-0.4	0.04	0.05	-	-	-	-
Obtained	0.0726	0.0197	0.148	0.0185	0.0166	0.0421	0.0104	0.03	Bal.

\* The Standard steel according to ASTM A568

**Fig. 1. Spot-welded lap joint configuration.**

For welding operation, a resistance spot welder machine (Miller Electric's SSW-2020), made in the US, was used to perform the weld. Before welding, all dirt and contamination were eliminated, and the specimens were cleaned completely with acetone. In the beginning, the weld was performed without the coating to choose the best welding conditions that would provide the best welding strength and obtain pullout failure mode without reaching the nugget expulsion as possible. Several trail tests were carried out using various variables of welding current and time. The welding parameters applied are shown in Table 4. Following the selection of the best welding conditions, zinc and tin coatings were applied to the base metals to study the coating effect on weldability and mechanical characteristics of the dissimilar welded joint. The summary of welding procedure is described in Fig. 2. To analyze the joint properties, the weldments were cut at the weld nugget cross-section using a wire cut machine to conduct metallographic examination and microhardness testing. This was followed by the typical grinding and polishing processes. Grinding was conducted on the mounted specimens starting with sandpaper (400, 600, 800, 1000, 1200, 2000, and 2500) and then polishing by fine cloth with the diamond paste of  $3\ \mu$  and  $\text{Al}_2\text{O}_3$  solution, then rinsed in water. The samples were then

etched by immersing in a solution of Nital for 15 s, which consists of (2% mL HNO<sub>3</sub> and 98% mL Ethanol) for the carbon steel (Abass *et al.*, 2021). An optical microscope and secondary electron microscope (SEM) were used to investigate the microstructure.

**Table 4. Parameters for welding low carbon steel to AA6061.**

Welding current (kA)	Welding time (s)	Electrode force (kN)
2	0.2	12.2
4	0.2	12.2
6	0.2	12.2
8	0.2	12.2
2	0.4	12.2
4	0.4	12.2
6	0.4	12.2
8	0.4	12.2
2	0.6	12.2
4	0.6	12.2
6	0.6	12.2
8	0.6	12.2
2	0.8	12.2
4	0.8	12.2
6	0.8	12.2
8	0.8	12.2
4	1	12.2
8	1	12.2

## 2.2. Tensile shear test

Computer controlled electronic universal testing machine, model (UE3450) with a (50) KN maximum capacity. The crosshead speed in this test was 1 mm/min.

## 2.3. Optical Microscopy

The optical microscopy NMM-800RF, with a magnification of (3201600) X with a digital camera connected to a computer, China). To examine the microstructure of low carbon steel.

## 2.4. Scanning Electron Microscopy and EDS

Scanning electron analysis type thermo scientific axia (inspect F 50, USA) at an accelerating voltage of 30 kV and spot size of 3. In secondary electron imaging mode and backscattered

mode to observe the microstructural of best welding conditions, with and without coating, and to study the elemental distribution in welding joint by using Energy Dispersive X-ray Spectrometry (EDS) attached with the SEM, the location of test in area mapping.

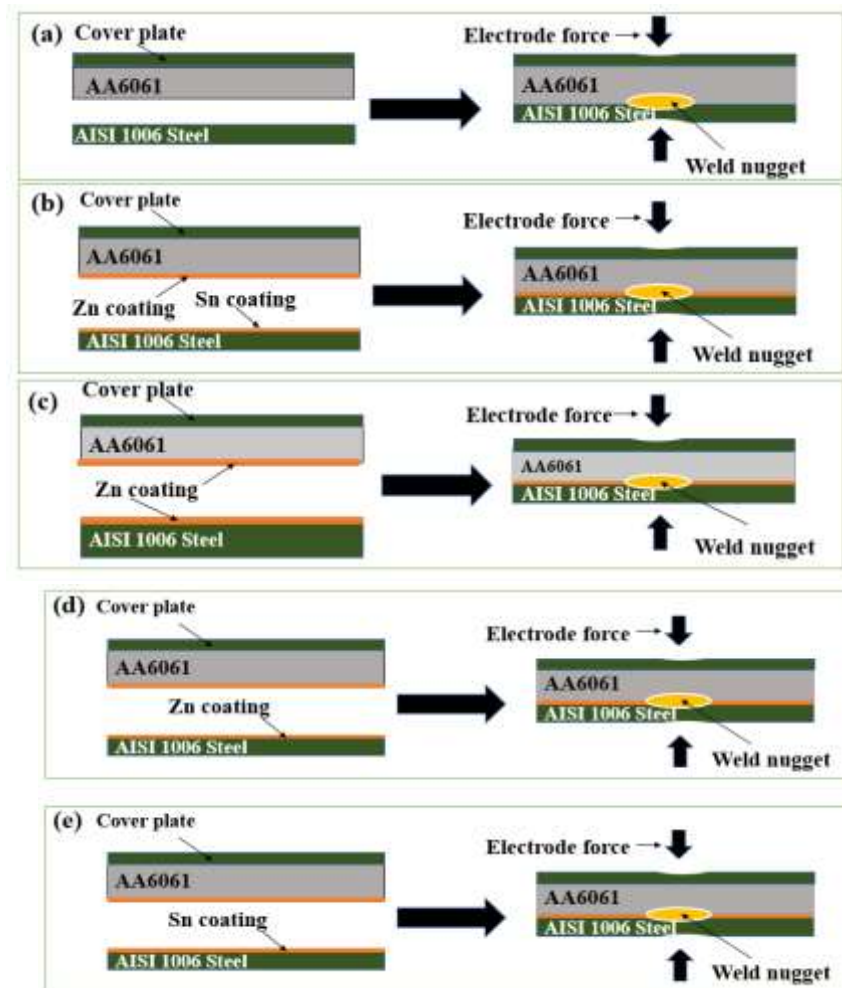


Fig. 2. Welding procedure for the samples (a) as weld (b) Sn coated St to Zn coated Al (c) Zn coated St to Zn coated Al (d) Zn coated St to Al (e) Sn coated St to Al.

### 2.5. Microhardness test

Testing the cross-section of welded joints, by using a Vickers hardness device type (TH715, Digital Micro Vickers hardness tester, made in China). It is supplied with microscope lenses of a total magnification of 400 X, Vickers Micro-hardness measurements were taken along a contour line for various one-side positions of the spot weld cross-section by utilizing 1.9 N load for aluminum alloy and 9.8 N load for low carbon steel for 15 s.

## 3. RESULTS AND DISCUSSION

### 3.1. Failure mode at the joint area

Welding conditions and weld nugget size directly impact failure mode in RSW. During low welding current, the weld nuggets size is small and has increased with the increasing welding current, as shown in Table (5). Failure types are introduced in Figure 3. Due to the relatively small nugget size, the joints welded with low welding currents i.e., 2 and 4 kA, failed in the interfacial failure (IF) mode, as illustrated in Fig. 3 (a). As the welding conditions (welding current and welding time) increase, the weld strength increases, and the failure mode change from interfacial to pullout. Fig. 3 (b) and (c) show a partial pullout failure (PF) mode where the fracture occurs in the aluminum nugget, and so does an explosion because of the relatively high heat input generated and the low melting temperature of aluminum relative to steel. The explosion phenomenon is undesirable as it can cause thinning of the aluminum and result in reduced mechanical properties (Chen *et al.*, 2019). The failure in Fig. 3 (d) was full pullout failure mode that occurs via complete nugget withdrawal from one sheet.

**Table 5. Effect welding parameters on nugget diameter.**

Welding current (kA)	Welding time (s)	Nugget diameter (mm)
4	0.6	4
6	0.6	5
8	0.6	6.5
8	1	7.5

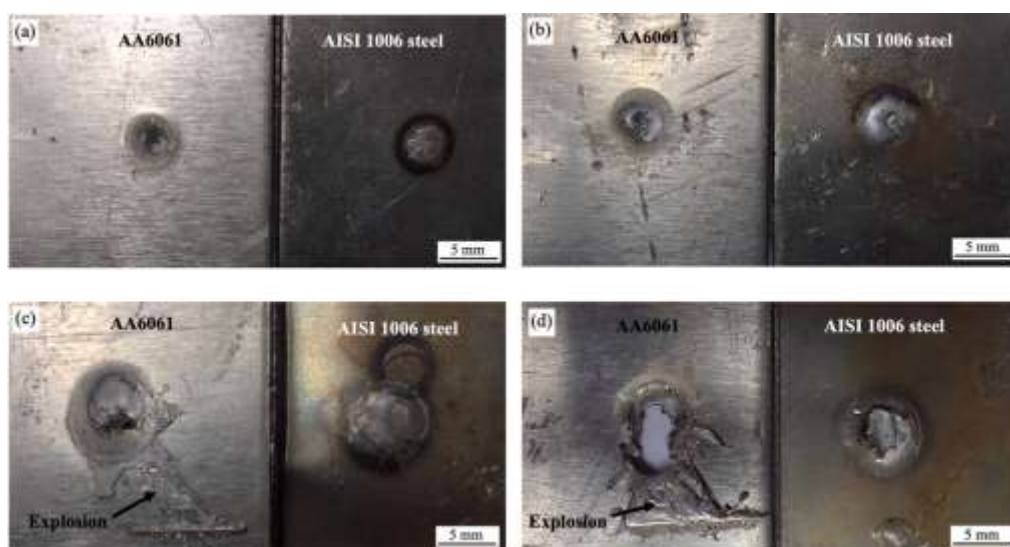


**Fig. 3. Failure modes of RSW joints. (a) IF at 4 kA, 0.6 s. (b) Partial PF at 6 kA, 0.6 sec. (c) Partial PF at 8 kA, 0.6 s. (d) Full PF at 8 kA, 1 s.**

### 3.2. Joint Strength

The quality of the joint was verified by performing a tensile shear strength test on the welded samples, and the influence of the RSW process parameters on shear strength was investigated. Table 5 shows the results of the tensile shear test of AISI 1006 steel /AA6061 with variations in welding current, welding time, and coating type. Welding conditions (6 KA, 0.6 sec) and (8 KA, 0.4 sec) were used because they gave a strong weld (approved by first weld trails) with limited explosion and crack. The results showed that when 6 KA current was used, the shear force was greater than 8 KA current, through which 6 KA current was chosen as the best welding condition. This can be attributed to the expulsion of molten aluminum at the joint area and also to the fact that with the increase in the welding current, the thickness of the reaction layer between the steel and aluminum increases including a higher amount of IMC due to the higher interfacial temperature of liquid Al alloy with solid steel (Zhang, Weihua, 2011). The formation of thick brittle Al-Fe intermetallic compounds has a negative effect on the tensile and shear strengths of the weld (Rahimi and Movahedi, 2020). Moreover, the high welding current causes the existence of some defects that negatively affect the joint strength, such as the production of distorted weld, and the presence of solidification cracking in the weld nugget, as presented in Fig. 4. To limit the growth of brittle IMCs and improve the joint quality, different types of coating were applied to the steel and aluminum base metals, such as tin-coated steel, zinc-coated aluminum, and zinc-coated steel. It was observed that the shear force slightly increased after applying the coating, where an increase was obtained 64% in the joint of tin-coated steel with zinc-coated, 17% in the joint zinc-coated steel to aluminum, and 8% in the joint of zinc-coated steel to zinc-coated aluminum, as illustrated in Fig. 5. It has been observed that the presence of an interlayer between aluminum and steel decreases the thermal expansion mismatch between the substrates during welding by melting and evaporating the coating layer and thereby consuming some of the heat available at the interface region (Arghavani, M. R., M. Movahedi, 2016). This indicates that the addition of coating had a positive effect on the shear force of some joints compared to as-welded joints without coating under the same welding conditions by producing a thinner layer of IMC as presented in Fig. 6.

### 3.3. Microstructure examination

At the interface region of the AA6061/AISI 1006 steel joint, the microstructure featured a clear bonding between the two dissimilar metals, especially with utilizing of coating as presented in Fig.7 and 8. During the RSW of steel to aluminum, the temperature at the steel and aluminum interface is higher than the melting point of the aluminum alloy and lower than the melting

point of the steel, and hence, the welding procedure included wetting and spreading liquid aluminum alloy over solid steel at the interface. Thus, the Al/steel connection is a liquid/solid interface, indicating that the metallurgical bonding of Al/steel using RSW is accomplished through a brazing process (Li *et al.*, 2022).

**Table 5. Results of tensile shear force of AISI1006 /AA6061 joints.**

RSW condition No.	Current (kA)	Welding time (s)	Tensile Shear load (kN)	Conditions
1	8	0.4	1.9	without coating
2	8	0.4	2.1	without coating
3	6	0.6	2.04	without coating
4	6	0.6	2.7	without coating
5	6	0.6	2.3	without coating
6	6	0.6	4.24	Sn coated St to Zn coated Al
7	6	0.6	3.62	Sn coated St to Zn coated Al
8	6	0.6	3.7	Sn coated St to Zn coated Al
9	6	0.6	2.6	Zn coated St to Al
10	6	0.6	2.82	Zn coated St to Al
11	6	0.6	2.8	Zn coated St to Al
12	6	0.6	2.4	Zn coated St to Zn coated Al
13	6	0.6	3	Zn coated St to Zn coated Al
14	6	0.6	2.52	Zn coated St to Zn coated Al
15	6	0.6	1.7	Sn coated St to Al
16	6	0.6	2.61	Sn coated St to Al
17	6	0.6	2.35	Sn coated St to Al

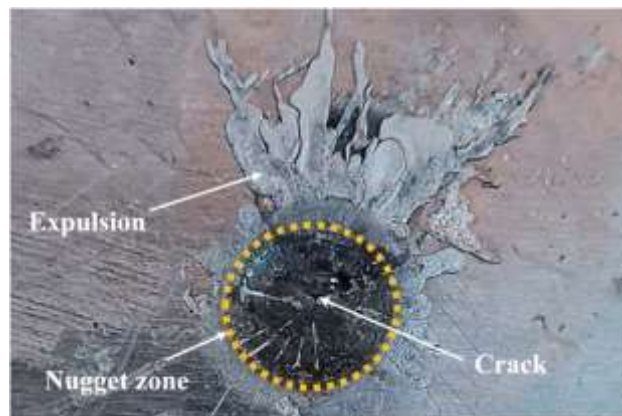


**Fig. 4. Weld nugget at Al side for RSW condition (8 kA, 0.6 s).**

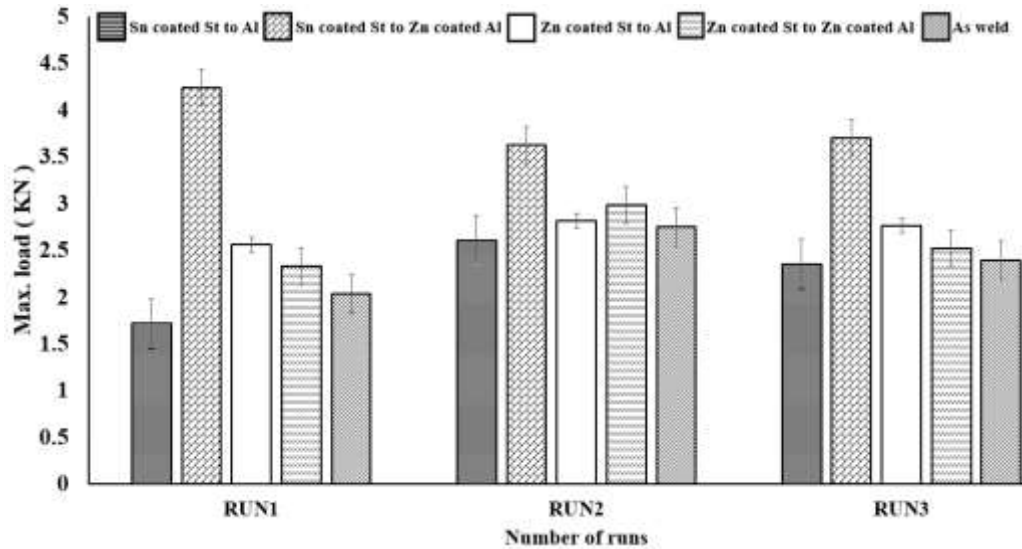


Fig. 5. Results of Shear forces for RSW condition (6 kA, 0.6 s).

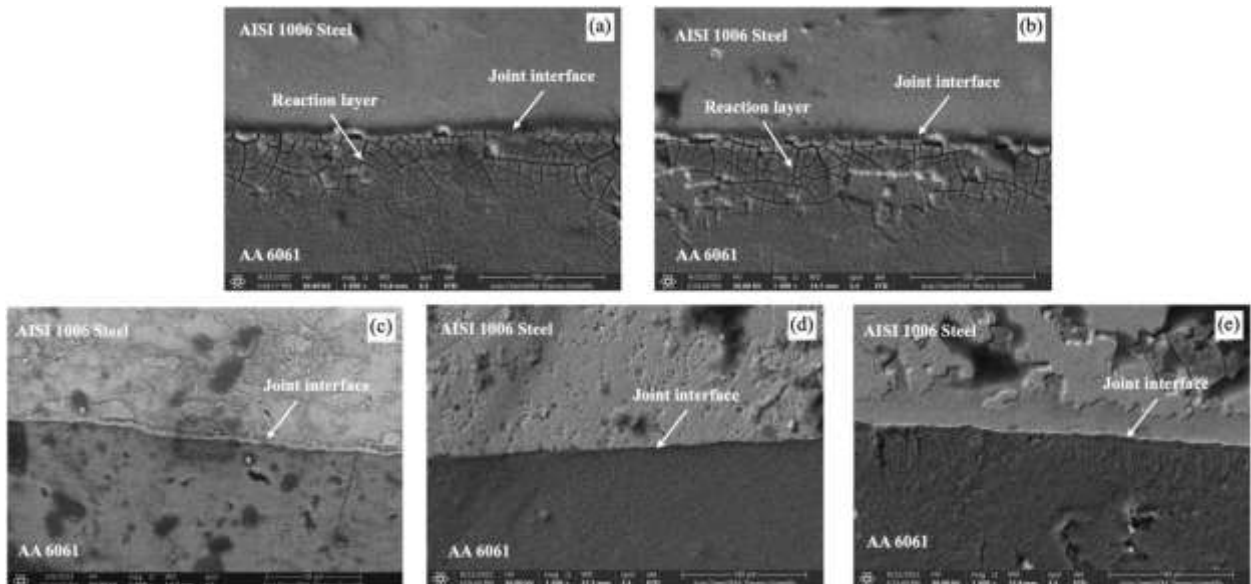
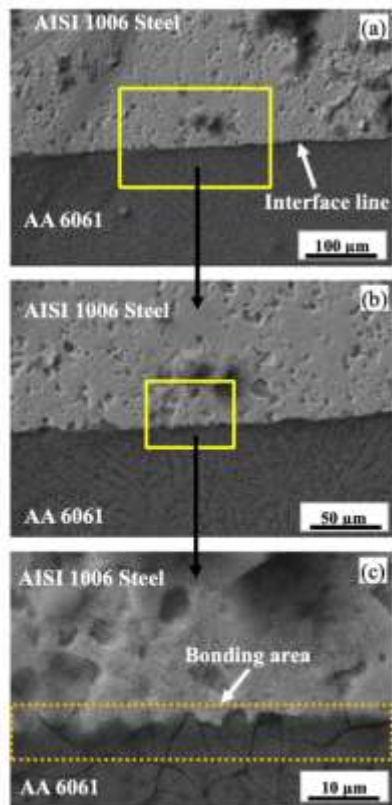
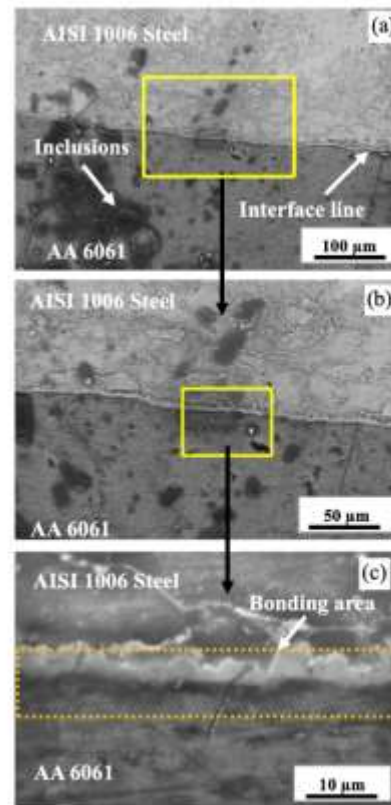


Fig.6. Joint interface and reaction layer at (6 kA, 0.6 s) welding parameters and different coating conditions. (a) As-welded (b) Sn coated St to Al (c) Sn coated St to Zn coated Al (d) Zn coated St to Zn coated Al (e) Zn coated St to Al



**Fig. 7. The SEM micrograph for Zn-coated steel / Zn-coated Al joint**



**Fig. 8. The SEM micrograph for Sn-coated steel / Zn-coated Al joint**

Fig. 9 shows the SEM images obtained from the AISI 1006 steel Sn-coated to AA606 zinc-coated interface regions showing the formation of the FeAl intermetallic compounds. The EDS analysis was performed at the interface region for the joints at different coating conditions. An example of EDS analysis is presented in Fig. 10 showing the dominating of Al and Fe in this area. Also, to ensure the presence of coating in the welding zone, where the presence of coating was observed in low percentages due to the evaporation of the coating layer during welding. The formation of the Fe-Al IMC layer reduces the joint strength and gives rise to the initiation and propagation of cracks as shown in Fig. 11. Thus, it is hard to achieve a perfect joint between these types of materials. Porosities are also defects that usually arise during the welding of aluminum, which are caused by the solubility of hydrogen. Hydrogen can come from the base metal, environment, and air. The solubility of hydrogen increases with increasing temperature and consequently increases the formation of the porosities (Ardika *et al.*, 2021).

On the steel side, the welding joint also showed a microstructural change in the steel. Fig. 12b shows the microstructure of the AISI 1006 steel base metal region (BM) consisting of pearlite and ferrite. Near the weld nugget, the microstructure was affected by welding heat and generated a HAZ with finer microstructure and an increase in pearlite which might be due to the migration of carbon to this area due to the heat effect as shown in Fig. 12c. Further toward

the weld nugget and due to higher heat and plastic deformation induced by electrode pressure, a thermo mechanically affected zone (TMAZ) is formed as presented in Fig. 12d. This change has an impact on the steel's mechanical properties.

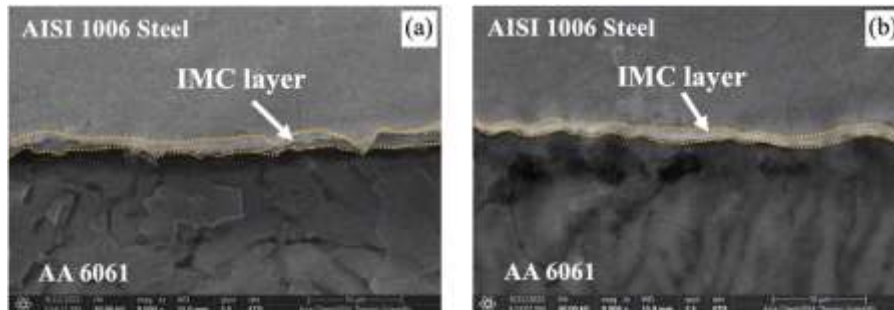


Fig. 9. The SEM micrograph for (a) Sn-coated steel / Zn-coated Al (b) Zn-coated steel / Al joint.

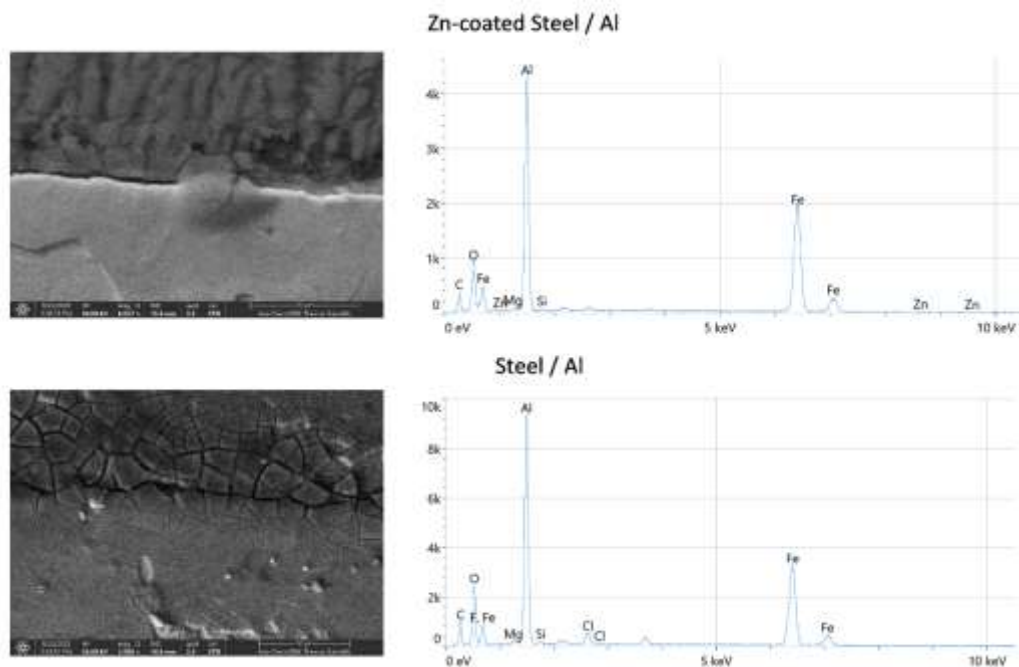


Fig. 10. The SEM micrograph with EDS analysis for Zn-coated steel / Al joint and Steel / Al joint

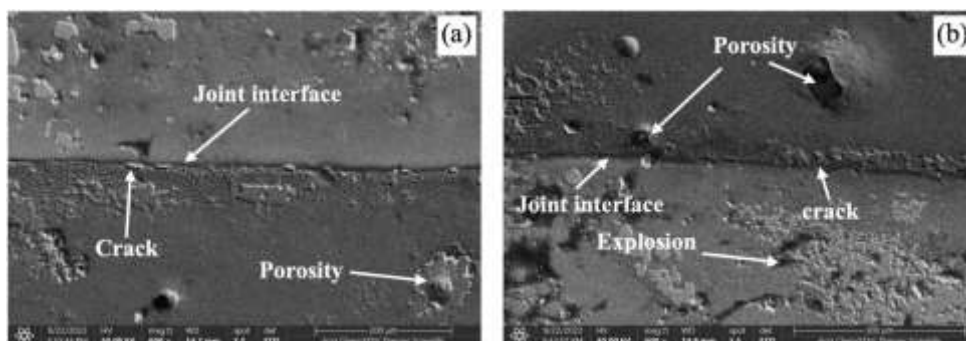
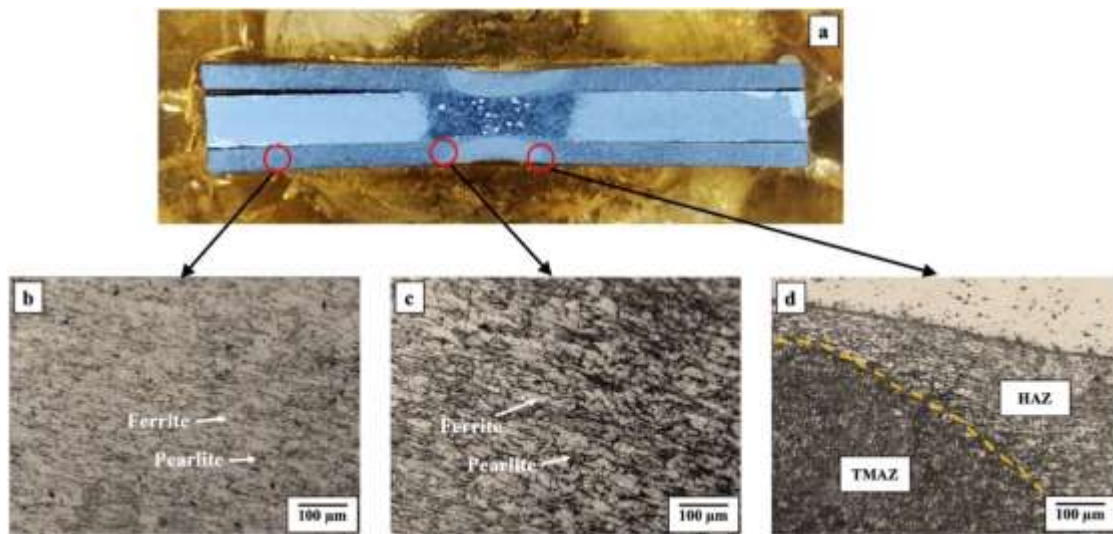


Fig. 11. The SEM micrograph for (a) Sn-coated steel / Al joint (b) As-weld.

### 3.4. Microhardness test

The hardness of the welded joints was evaluated using Vickers microhardness test. The tested joints were welded with 6 kA, 0.6 s welding parameters at different coating conditions. The test covered the BM zone, HAZ, and nugget zone. The tested locations are represented by five circles in Fig. 13. The microhardness of BMs was examined in order to gain an understanding of how the heat generated during welding affects the material mechanical properties. The average microhardness of aluminum and steel BMs (regions 1 and 2) were 41 and 120 HV respectively.



**Fig. 12. Optical Microstructures of AISI 1006 steel side.**

At the HAZs, aluminum (region 3) showed a slightly lower hardness than the BM with an average of 37 HV, which could be due to the effect of welding heat that caused overaging or dissolution of strengthening precipitates (Manladan *et al.*, 2017). Regarding the HAZ of AISI 1006 steel (region 4), the microhardness test recorded a slight decrease compared to BM due to the limited change in the microstructure of the HAZ as shown in Fig. 12.c, where the average hardness reached 115 HV, which is possibly due to the stress relief in this region induced by the welding heat (Kadhim, 2016). At the nugget zone (region 5), in spite of the nugget zone consisting of aluminum, the average hardness value was significantly higher than aluminum BM and HAZ with 106 HV. The reason for the hardness rising in Region 5 might be related to the existence of some IMC dispersed in the weld nugget resulting from the highest amount of welding heat and pressure in this area, As shown in Fig. 9. It was also observed that the HV value at region 5 was also affected by the coating condition. The existing coating slightly raised the hardness to that without coating from 99 HV to 110 HV, as presented in Fig. 13. The slight

increase in hardness can be related to the effect of alloying elements resulting from the coating that enhanced the hardness in the welded region (Tosun, 2012).

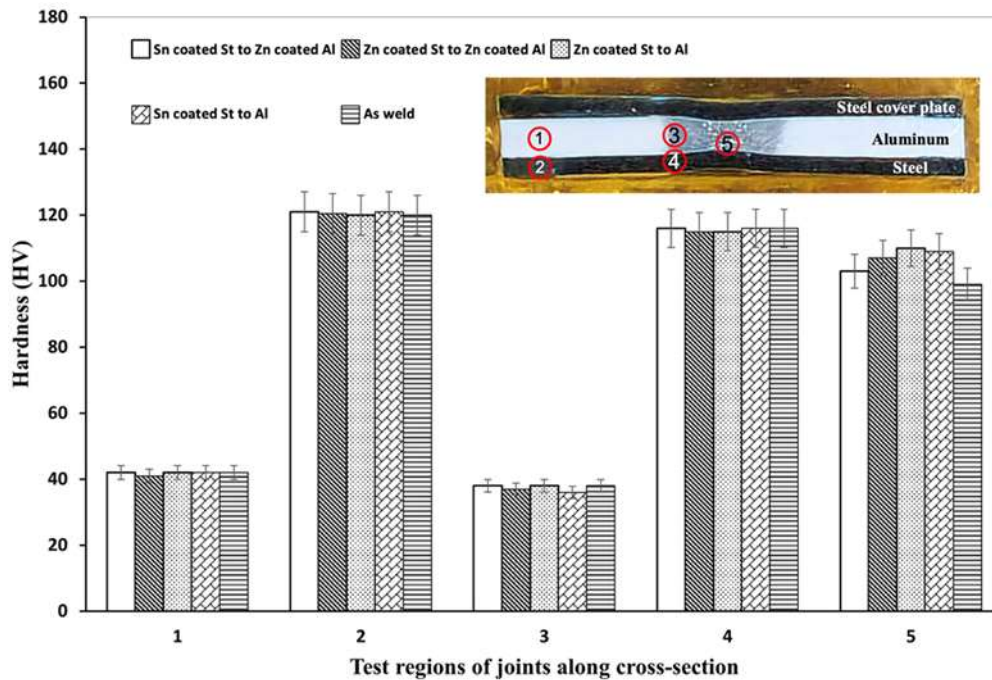


**Fig. 13. Results of Vickers hardness of cross-section of AISI 1006 Steel /AA6061 joint at best welding condition.**

#### 4. CONCLUSION

The following points can be concluded from this work:

1. Low welding current produced interfacial failure mode. When the welding current increases, the failure mode changes from interfacial to partial pullout and full pullout failure modes.
2. The best welding parameters for as-welded samples were 6 kA and 0.6s, where the maximum shear force of 2.7 kN was obtained.
3. With the utilization of a coating, the shear force increased, as the highest shear force of 4.25 kN achieved a 57% increment.
4. A clear bonding was obtained and detected by the SEM between the steel and aluminum, especially with the coated base metals.
5. The weld nugget consisted of aluminum since the welding of steel to aluminum is made through a brazing mechanism.
6. The existence of IMCs at the joint interface reduced the joint strength and cracks occurred at the interface region.

7. The microhardness was affected by the heat of welding and consequently varied across the joint, and an increase in the weld nugget was obtained because of the IMC effect.

## **5. REFERENCES**

- Abass, M.H. et al. (2021) 'Mechanical Properties and Microstructure Evolution in Arc Stud Welding Joints of AISI 1020 with AISI 316L and AISI 304', *Metallography, Microstructure, and Analysis*, 10(3), pp. 321–333.
- Ardika, R. et al. (2021) 'A review porosity in aluminum welding', *Procedia Structural Integrity*, 33, pp. 171–180.
- Arghavani, M. R., M. Movahedi, and A.H.K. (2016) 'Role of zinc layer in resistance spot welding of aluminium to steel', *Materials & Design*, pp. 106–114.
- Chen, C. et al. (2019) 'The robustness of Al-steel resistance spot welding process', *Journal of Manufacturing Processes*, 43, pp. 300–310.
- Chen, N. et al. (2018) 'Microstructural and mechanical evolution of Al/steel interface with Fe<sub>2</sub>Al<sub>5</sub> growth in resistance spot welding of aluminum to steel', *Journal of Manufacturing Processes*, 34, pp. 424–434.
- Das, T., Das, R. and Paul, J. (2020) 'Resistance spot welding of dissimilar AISI-1008 steel/Al-1100 alloy lap joints with a graphene interlayer', *Journal of Manufacturing Processes*, 53, pp. 260–274.
- Fang, Y. et al. (2019) 'A review on dissimilar metals' welding methods and mechanisms with interlayer', *International Journal of Advanced Manufacturing Technology*, 102(9–12), pp. 2845–2863.
- Gullino, A. et al. (2019) 'Review of aluminum-to-steel welding technologies for car-body applications', *Metals*, 9, p. 315.
- Kadhim, Z.D. (2016) 'Effect of quenching media on mechanical properties for medium carbon steel', *Int. Journal of Engineering Research and Application*, 6, pp. 26–34.
- Li, M. et al. (2022) 'Hybrid resistance-laser spot welding of aluminum to steel dissimilar materials: Microstructure and mechanical properties', *Materials & Design*, 221, p. 111022.
- Manh, N.Q. (2016) 'Dissimilar joining a6061 aluminum alloy and Sus304 stainless steel by the Tungsten Inert Gas welding process', *Vietnam Journal of Science and Technology*, 54(5A), pp. 64–74.

- Manladan, S.M. et al. (2017) 'A review on resistance spot welding of aluminum alloys', *International Journal of Advanced Manufacturing Technology*, 90(1–4), pp. 605–634.
- Prabakaran, R. et al. (2017) 'Synthesis and characterization of high entropy alloy (CrMnFeNiCu) reinforced AA6061 aluminium matrix composite', *J. Mech. Mechan. Eng.*, 21, pp. 415–424.
- Rahimi, S. and Movahedi, M. (2020) 'Resistance Spot Welding of Aluminum to Aluminum Clad Steel Sheet: Experimental and Theoretical Analysis', *Journal of Manufacturing Processes*, 58, pp. 429–435.
- Rajesh Jesudoss Hynes, N., Nagaraj, P. and Angela Jennifa Sujana, J. (2014) 'Mechanical Evaluation and Microstructure of Friction Stud Welded Aluminium-Mild steel Joints', 39(6), pp. 5017–5023.
- Ren, Daxin, et al. (2018) 'Clinch-resistance spot welding of galvanized mild steel to 5083 Al alloy', *The International Journal of Advanced Manufacturing Technology* 2018 101:1, 101(1), pp. 511–521.
- Sharma, H. et al. (2022) 'Investigation of mechanical and erosive behaviour of the Al 6061-SiC composites fabricated by stir casting', *Materials Today: Proceedings*, 69, pp. 446–453.
- Singh, J., Arora, K.S. and Shukla, D.K. (2019) 'Dissimilar MIG-CMT weld-brazing of aluminium to steel: A review', 783, pp. 753–764.
- Šut'ák, D. et al. (2020) 'Simulation of rifled tubes drawing process', *IOP Conference Series: Materials Science and Engineering*, 776(1), pp. 12–51.
- Tosun, G. (2012) 'Ni–WC coating on AISI 1010 steel using TIG: Microstructure and microhardness', *Arabian Journal for Science and Engineering*, 39(3), pp. 2097–2106.
- Zhang, Weihua, et al. (2011) 'Characterization of intermetallic compounds in dissimilar material resistance spot welded joint of high strength steel and aluminum alloy', *Isij International*, 51(11), pp. 1870–1877.